analytical chemistry

pubs.acs.org/ac Letter

Imaging with Ion Channels

Cheng Zhu,[‡] Kaixiang Huang,[‡] Yunong Wang, Kristen Alanis, Wenqing Shi, and Lane A. Baker*

Cite This: *Anal. Chem.* 2021, 93, 5355−5359 Read Online

ACCESS | Metrics & More | Article Recommendations | Supporting Information

ABSTRACT: We describe the incorporation of gated ion channels into probes for scanning ion conductance microscopy (SICM) as a robust platform for collecting spatial information at interfaces. Specifically, a dual-barrel pipet is used, where one barrel controls the pipet position and the second barrel houses voltage-gated transient receptor potential vanilloid 1 (TRPV1) channels excised in a sniffer-patch configuration. Spatially resolved sensing with TRPV1 channels is demonstrated by imaging a porous membrane where a transmembrane potential across the membrane generates local electric field gradients at pores that activate TRPV1 channels when the probe is in the vicinity of the pore. The scanning routine and automated signal analysis demonstrated provide a generalizable approach to employing gated ion channels as sensors for imaging applications.

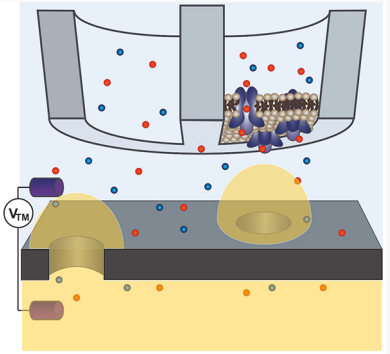

Conceptually, the use of proteins to form nanopores has provided an intriguing platform for the development of new approaches to chemical and biochemical sensing. For example, nucleic acid sequencing by protein nanopores has proven to be a disruptive technology in the area of genomics.[1,2] The majority of sensing platforms designed around protein nanopores have taken advantage of bacterial pore forming toxins such as α-hemolysin that assemble spontaneously into membranes and bilayers to form channels.[3−5] These pore forming toxins typically rely on β barrel structures where genetic manipulation of channel dimensions or chemistries has been used to demonstrate sensing platforms with both an extraordinary range of target analytes and exquisite selectivity.

Protein nanopores can also be based on gated ion channels, where the state of the channel, opened or closed, can be induced by external stimuli, including mechanical forces, temperature, voltage, and specific chemistries.[5,6] In this respect, gated ion channels prove especially intriguing as they possess an inherent sensing mechanism for chemical or physical properties. However, gated ion channels often prove more difficult to work with, typically having more complex structures and gating mechanisms subject to additional factors, such as lipid composition or accessory proteins. For these reasons, the use of gated ion channels in sensing platforms has been less prevalent than other types of protein nanopores. Sniffer-patches prove perhaps the most intriguing example of gated ion channel sensors that has been intermittently examined over the last few decades.[7−10] A sniffer-patch is formed at the tip of a glass pipet by gentle suction to extract a piece of cell membrane from a donor cell. If the extracted cell membrane contains an ion channel (or channels) and the extraction process results in the formation of the requisite gigaohm seal, the ion channel modified pipet can be used to form a sensor, where the ion channel serves as a recognition element and the flow of ions through the channel (between an electrode inside of the pipet and another one outside of the pipet) serves to transduce recognition. The sniffer-patch approach has been applied sparingly, most likely due to the fact that forming patches can be somewhat challenging and manipulating pipettes with excised channels in a physical space is often not straightforward.

In several recent reports, we have sought to use protein nanopores to imbue sensing attributes to pipettes suitable for use as probes in scanning ion conductance microscopy (SICM),[11,12] which we collectively describe as ion channel probes (ICPs).[13−15] Here, for the first time, we demonstrate an automated approach to imaging and signal analysis that allows the incorporation of gated ICPs combined with true scanning ion conductance microscopy feedback for selective imaging, therefore achieving a route to simultaneous maps of SICM topography and local information (chemical species, electric field, etc.).

The instrument setup used is illustrated in Figure 1. The ICP-SICM probe consists of a dual-barrel pipet (Figure 2b and S2) with transient receptor potential vanilloid 1 (TRPV1) channels incorporated into one of the barrels and the second barrel left open for SICM feedback control. TRPV1 is known as a voltage-gated ion channel that can be activated by external potentials.[16] A porous polyimide (PI) membrane mounted

Received: January 17, 2021
Accepted: March 16, 2021
Published: March 24, 2021

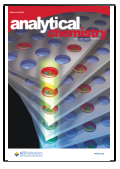

https://doi.org/10.1021/acs.analchem.1c00224
Anal. Chem. 2021, 93, 5355−5359

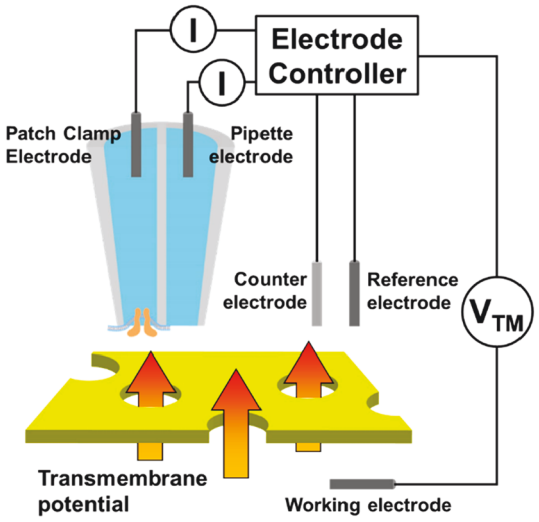

Figure 1. Schematic of membrane patch-ion channel probes (ICPs) used for scanning ion conductance microscopy (SICM) imaging in the experiments. Voltage gating of transient receptor potential vanilloid 1 (TRPV1) receptor is used to report on the location of local electric fields through a porous membrane.

between two halves of a perfusion cell separates chambers filled with an electrolyte solution.[17] The working electrode (Ag/AgCl) in the bottom chamber is used to apply a transmembrane potential (V_{TM}), generating a potential field over pores in the membrane (Figures 2a and S1). An electrode (pipet electrode) inserted inside one barrel of the dual-barrel pipet (Figure 2b) serves as an SICM electrode, monitoring a distance-dependent ion current to control the probe position. The second barrel of the pipet (patch-clamp electrode) houses an excised sniffer-patch containing TRPV1 channels from a donor cell (Figure S3) and records the gating of the TRPV1 channel via the amperometric current−time ($I-T$) response. All electrodes reference a common reference electrode (RE; Ag/AgCl) in the top chamber, and a counter electrode (Pt) avoids potential deflection of the RE (Figure S4). A modified scan protocol based on the hopping mode[18] was enabled via a field programmable gate array to orchestrate the application of the potential and recording of the current at the multiple electrodes used.[19] After the pipet approached the surface, the feedback of SICM was paused for a fixed time, during which the scan potential was turned off and V_{TM} was applied. At the same time, the $I-T$ response of the patch-clamp barrel was recorded, which reports (in this case) on the changes in electric fields at the surface of the PI membrane. After measurement, V_{TM} was turned off and the scan potential was turned back on; the pipet was retracted, moved to the next pixel, and reapproached to the surface (see Figure S5 for typical traces of the scan potential, V_{TM}, and voltages applied on the X, Y, and Z piezoelectric positioners during scanning). The process was repeated iteratively to build up a data set that resolves both topography and ion channel activity.

Sensing the electric field over the pores with TRPV1 channels was first demonstrated in the most straightforward manner by changing V_{TM} to modify the potential field over a pore with ∼1.35 μm diameter (Figure 2c). For these measurements, the pipet was maintained at the same vertical position over a pore and V_{TM} was stepped from 3 to 8 V with an increment of 1 V. As V_{TM} was stepped up, the open probability (P_{open}) of the TRPV1 channels, an indicator of channel activity, also increased gradually from 16% to 54% with more complex states observed at a higher V_{TM} (discussed below).

The sensitivity of the TRPV1 ion channel to local potential change can also be demonstrated by performing a distance-dependent $I-T$ measurement (results shown in Figure S8). Briefly, after the pipet reached the closest approach, the pipet was retracted by 1 μm and manually positioned to the center of the pore. This position was labeled as the initial point (0 position) and used as the reference for distances indicated below. A constant V_{TM} of 2 V was then applied, and the $I-T$ response of the membrane patch was recorded. The pipet was further approached by 200 nm by piezo, and another $I-T$ response was measured again under the same conditions. This process was repeated until a pronounced ion channel response was observed (at 800 nm from the initial point). When the pipet was placed at positions relatively far away from the pore (position 0 and 200 nm), the $I-T$ traces showed a similar open-state current (I_{open}) of ∼1.2 pA. P_{open} was also maintained at a relatively low level (<10%). I_{open} increased as the pipet was approached to the pore and reached 6 pA at 800 nm. P_{open} also increased significantly and reached 26% at 800 nm. Starting at 600 nm, a second open state was observed on the $I-T$ traces with twice the magnitude of the first open state, which is due to the simultaneous activation of two ion channels. At 800 nm, an intermediate open state was observed (green dashed line), which may be related to the activation of

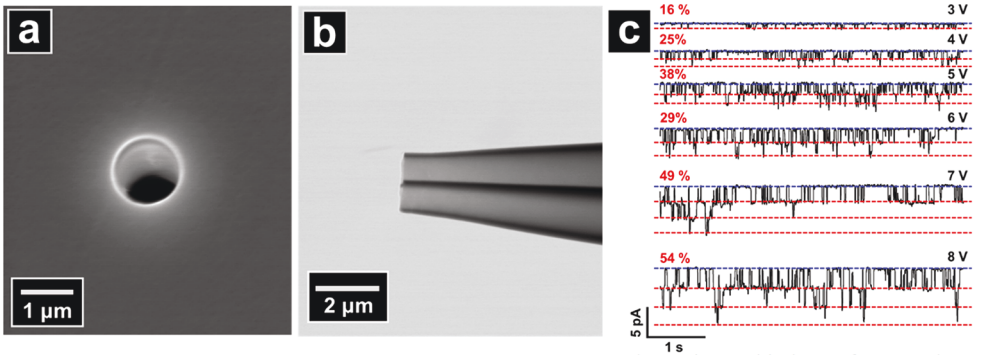

Figure 2. (a) Electron micrograph (EM) of the pore in a polyimide membrane imaged in the lower frames. (b) EM of a typical pipet used for imaging. (c) The open probability and representative $I-T$ traces of a membrane patch when the pipet was positioned over a pore under different transmembrane potentials.

https://doi.org/10.1021/acs.analchem.1c00224
Anal. Chem. 2021, 93, 5355−5359

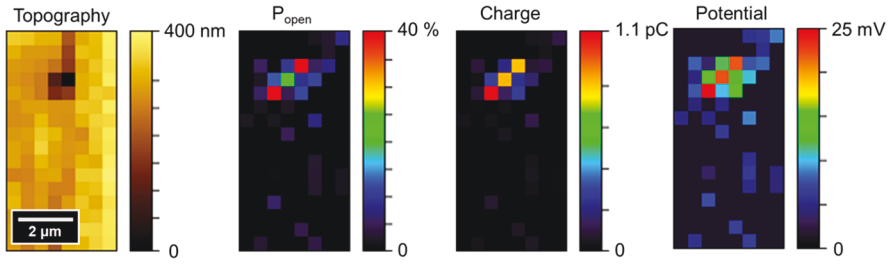

Figure 3. Topography, open probability, charge, and the local potential map of a single pore with a diameter of ∼1.35 μm collected by the ICP-SICM scan protocol.

native ion channels in HEK cells or an intermediate state of TRPV1 ion channels.

To demonstrate the feasibility of using TRPV1 channels as a sensor for local potential mapping, an area with a single pore was selected and imaged with the aforementioned scan protocol (V_{TM} = 800 mV), recording both topography and ion channel response. The $I-T$ trace at each pixel was then analyzed with an event detection MATLAB script (see Section S2), from which P_{open} was calculated and plotted with XY-coordinates to generate the P_{open} map. P_{open} has a nominally linear relationship with the applied membrane potential under a certain potential range for the TRPV1 channels.[20,21] However, using P_{open} for quantifying local potential only works well for the membrane patches with a single ion channel. For membrane patches bearing multiple ion channels, each ion channel may be excited by the potential independently and generate an open event with the same I_{open}. As a result, membrane patches with multiple channels usually have a significantly higher P_{open}. Moreover, P_{open} would saturate easily at high potentials, causing a loss of sensitivity. To more accurately characterize local potential, charge (i.e., ions) passing through the membrane patch were also calculated by integrating I_{open} with the recording time. The charge values were plotted with XY-coordinates to generate a charge map. The SICM topography image, the P_{open} map, and the charge map of a ∼1.35 μm pore are shown in Figure 3 (left three images). The pore could be clearly identified in the topography image shown as the lower features. The position of the pore matches well with that visualized in both P_{open} and charge images, suggesting a stronger electric field above the pore area. The resolution of the topography image was relatively low compared to typical SICM imaging since a larger probe was used here. Compared to P_{open}, the changes in charge were more pronounced since the charge includes information of both P_{open} and I_{open}. The charge value can be further converted to a local potential with the relationship between V_{TM}, P_{open}, and I_{open}. Both P_{open} and I_{open} are proportional to the membrane potential at potentials smaller than 100 mV.[22,23] Since the charge transferred through the membrane is proportional to both P_{open} and I_{open}, the charge would then be proportional to the square of the membrane potential. Therefore, the magnitude of the local potential can be derived from the charge value. The charge−potential relationship of the membrane patch was calibrated either before or after scanning, where the ion channels were activated by directly applying a membrane potential on the patch-clamp electrode. The resultant $I-T$ responses of the membrane patch were then recorded at different potentials to give a relatively linear calibration curve from plotting the square root of the charge with the membrane potential (Figure S7). With the calibration curve, the charge image can then be turned into a local potential map, as shown in Figure 3 (right).

Additionally, the changes in electric field were measured on an area with multiple pores. The P_{open}, charge, and the corresponding topography image are shown in Figure 4b−d.

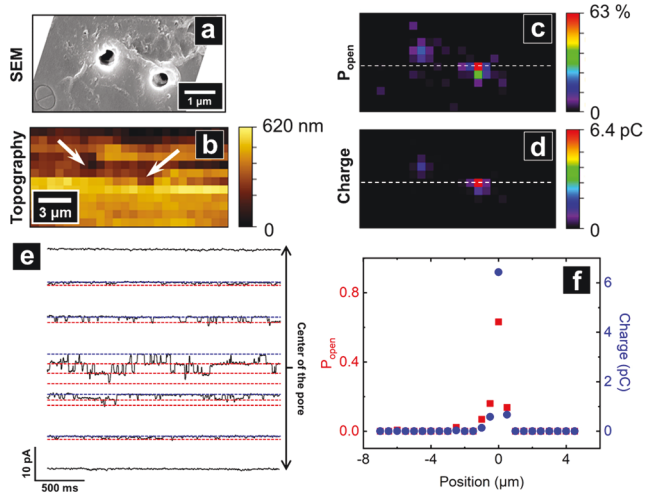

Figure 4. (a) Scanning electron micrograph of two pores imaged after performing ICP-SICM measurements. Note the lower left shows the impression made from advancing the tip into the membrane surface. (b, c, d) The topography, open probability, and charge maps of the pores shown in (a). (e) The $I-T$ traces of the pore center (middle) and three pixels adjacent to it at each side. (f) Line profiles of open probability and charge that pass through the center of a pore (highlighted with white lines in (c) and (d)). The center pixel of the pore was set as 0.

The scan area was imaged with electron microscopy (Figure 4a) and showed good correlation with P_{open} and the charge images. The shape of the pipet was also imprinted onto the membrane by hopping the pipet with a high threshold (20% of steady-state current), which can be visualized in the electron micrograph (bottom left corner). The magnitude of changes in P_{open} and the charge passed through the membrane can be more clearly depicted in Figure 4e and the line profiles (Figure 4f), where the center of the pore was set as the origin. Both P_{open} and charge transferred through the membrane patch were significantly higher immediately over the pore.

Spatial distribution of the local potential over a ∼2.56 μm pore (Figure S9) was investigated in addition to the 1.35 μm pore (Figure 3), in which the maximum potential was ∼25 mV over the 1.35 μm pore and ∼89 mV over the 2.56 μm pore. The measured potential near the 1.35 μm pore was close to the simulated results (21 mV) under the same conditions (Figures

https://doi.org/10.1021/acs.analchem.1c00224
Anal. Chem. 2021, 93, 5355−5359

S12−14). However, the measured potential near the 2.56 μm pore was much larger than the simulated result (37 mV). This discrepancy may be rationalized by the vertical position of the tip during measurement. For tip and pore sizes used here, the pipet tip needs to dip into the 2.56 μm pore to sense the surface, where the potential magnitude is much higher than positions just outside of the pore (Figure S12b). Additionally, P_{open}, charge, and the corresponding topography images of the same samples were also collected under a higher V_{TM} (Figures S10 and S11), in which the pores exhibited elevated charge values compared to V_{TM} = 0.8 V. This further demonstrates the ability of the TRPV1 channels to detect the local potential.

In conclusion, we have described a robust method for local potential mapping with ICP-SICM. The scan probe was constructed with a dual-barrel pipet, in which the ion channels inside the membrane patch were used as the sensor for local potential measurement. A perfusion cell was developed with a piece of porous polymer membrane, where a potential gradient can be generated near the pores under a transmembrane potential. A customized scan protocol was developed to automate the scanning of the pipet and the collection of the $I-T$ responses of the membrane patch after the pipet approached the sample surface. $I-T$ responses were then analyzed to generate P_{open} and charge passing through the membrane. Both values were plotted with XY-coordinates to generate images to qualitatively illustrate the potential distribution on the samples. The potential magnitude on the sample surface can be quantified by fitting the charge to a calibration curve to depict the relationship between the charge and membrane potential. In the future, this novel ICP-SICM platform can be utilized for label-free nanoscale mapping of specific chemical species in biological systems based on the activity of target ligand-gated ion channels, which can elucidate extracellular chemical concentrations.

■ ASSOCIATED CONTENT

Supporting Information

The Supporting Information is available free of charge at https://pubs.acs.org/doi/10.1021/acs.analchem.1c00224.

Details of the experimental procedures, simulations, and ICP-SICM results (PDF)

■ AUTHOR INFORMATION

Corresponding Author

Lane A. Baker − *Department of Chemistry, Indiana University, Bloomington, Indiana 47405, United States;* orcid.org/0000-0001-5127-507X; Phone: 812-856-1873; Email: lanbaker@indiana.edu

Authors

Cheng Zhu − *Department of Chemistry, Indiana University, Bloomington, Indiana 47405, United States*

Kaixiang Huang − *Department of Chemistry, Indiana University, Bloomington, Indiana 47405, United States*

Yunong Wang − *Department of Chemistry, Indiana University, Bloomington, Indiana 47405, United States*

Kristen Alanis − *Department of Chemistry, Indiana University, Bloomington, Indiana 47405, United States*

Wenqing Shi − *Department of Chemistry, Indiana University, Bloomington, Indiana 47405, United States*

Complete contact information is available at: https://pubs.acs.org/10.1021/acs.analchem.1c00224

Author Contributions

‡C.Z. and K.H. contributed equally to this work.

Notes

The authors declare no competing financial interest.

■ ACKNOWLEDGMENTS

The work was supported by the National Science Foundation grant CHE-1808133 and the National Institutes of Health (NIH) grant 5R01NS105888-03, and K.A. was supported by a fellowship from the Graduate Training Program Quantitative and Chemical Biology (QCB) at Indiana University (Grants T32 GM131994 and GM109825). Electronic Instrument Services at Indiana University is acknowledged for designing and building the electronic devices, including David Bancroft for programming. The IU Nanoscale Characterization Facility (NCF) is acknowledged for access to and use of the electron microscope.

■ REFERENCES

(1) Deamer, D.; Akeson, M.; Branton, D. *Nat. Biotechnol.* **2016**, *34*, 518−524.
(2) Escalona, M.; Rocha, S.; Posada, D. *Nat. Rev. Genet.* **2016**, *17*, 459−469.
(3) Bayley, H. *Curr. Opin. Chem. Biol.* **2006**, *10*, 628−637.
(4) Bayley, H.; Martin, C. R. *Chem. Rev.* **2000**, *100*, 2575−2594.
(5) Shi, W.; Friedman, A. K.; Baker, L. A. *Anal. Chem.* **2017**, *89*, 157−188.
(6) Tovar, K. R.; Westbrook, G. L. Chapter 31 - Ligand-Gated Ion Channels. In *Cell Physiology Source Book*, Fourth ed.; Sperelakis, N., Ed.; Academic Press: San Diego, CA, 2012; pp 549−562.
(7) Allen, T. G. J. *Trends Neurosci.* **1997**, *20*, 192−197.
(8) Christian, C. A.; Huguenard, J. R. *J. Neurophysiol.* **2013**, *110*, 1722−1731.
(9) Christensen, R. K.; Petersen, A. V.; Schmitt, N.; Perrier, J.-F. *Front. Cell. Neurosci.* **2014**, *8*, 133.
(10) Muller-Chrétien, É. Outside-Out "Sniffer-Patch" Clamp Technique for In Situ Measures of Neurotransmitter Release. In *Patch-Clamp Methods and Protocols*; Martina, M., Taverna, S., Eds.; Springer New York: New York, NY, 2014; Vol. *1183*, pp 195−204.
(11) Hansma, P. K.; Drake, B.; Marti, O.; Gould, S. A.; Prater, C. B. *Science* **1989**, *243*, 641.
(12) Zhu, C.; Huang, K.; Siepser, N. P.; Baker, L. A. Scanning Ion Conductance Microscopy. *Chem. Rev.* **2020**, DOI: 10.1021/acs.chemrev.0c00962.
(13) Zhou, Y.; Bright, L. K.; Shi, W.; Aspinwall, C. A.; Baker, L. A. *Langmuir* **2014**, *30*, 15351−15355.
(14) Shi, W.; Zeng, Y.; Zhou, L.; Xiao, Y.; Cummins, T. R.; Baker, L. A. *Faraday Discuss.* **2016**, *193*, 81−97.
(15) Shi, W.; Zeng, Y.; Zhu, C.; Xiao, Y.; Cummins, T. R.; Hou, J.; Baker, L. A. *Small* **2018**, *14*, 1702945.
(16) Nilius, B.; Talavera, K.; Owsianik, G.; Prenen, J.; Droogmans, G.; Voets, T. *J. Physiol.* **2005**, *567*, 35−44.
(17) Chen, C.-C.; Derylo, M. A.; Baker, L. A. *Anal. Chem.* **2009**, *81*, 4742−4751.
(18) Novak, P.; Li, C.; Shevchuk, A. I.; Stepanyan, R.; Caldwell, M.; Hughes, S.; Smart, T. G.; Gorelik, J.; Ostanin, V. P.; Lab, M. J.; Moss, G. W. J.; Frolenkov, G. I.; Klenerman, D.; Korchev, Y. E. *Nat. Methods* **2009**, *6*, 279−281.
(19) Zhou, L.; Gong, Y.; Hou, J.; Baker, L. A. *Anal. Chem.* **2017**, *89*, 13603−13609.
(20) Fischer, M. J. M.; Balasuriya, D.; Jeggle, P.; Goetze, T. A.; McNaughton, P. A.; Reeh, P. W.; Edwardson, J. M. *Pfluegers Arch.* **2014**, *466*, 2229−2241.
(21) de la Roche, J.; Walther, I.; Leonow, W.; Hage, A.; Eberhardt, M.; Fischer, M.; Reeh, P. W.; Sauer, S.; Leffler, A. *Sci. Rep.* **2016**, *6*, 36740.

(22) Hazan, A.; Kumar, R.; Matzner, H.; Priel, A. *Sci. Rep.* **2015**, *5*, 12278.
(23) Caires, R.; Luis, E.; Taberner, F. J.; Fernandez-Ballester, G.; Ferrer-Montiel, A.; Balazs, E. A.; Gomis, A.; Belmonte, C.; de la Peña, E. *Nat. Commun.* **2015**, *6*, 8095.

https://doi.org/10.1021/acs.analchem.1c00224
Anal. Chem. 2021, 93, 5355−5359